DEVELOPMENT OF A MECHANICAL TESTING ASSAY FOR FIBROTIC MURINE LIVER

By

Stephanie Lynne Barnes

Thesis

Submitted to the Faculty of the

Graduate School of Vanderbilt University

in partial fulfillment of the requirements

for the degree of

MASTER OF SCIENCE

in

Biomedical Engineering

May, 2007

Nashville, Tennessee

Approved:

Professor Michael I. Miga

Professor John Gore

AKNOWLEDGEMENTS

I would like to thank my advisor, Dr. Miga, for his guidance in this project and for the energy and excitement that he constantly exudes. His insight has been imperative to the development of this work. Thanks to Andrej Lyshchik, who managed the animal aspect of the research, among many other contributions. I would also like to thank Dr. Gore for his insight and the many resources he provided. Finally, thank you to the many people in VUIIS who helped with the imaging and lab resources, as well as the people in the histological analysis lab for preparing the tissue slides. This research was made possible by funding provided by the National Science Foundation Graduate Research Fellowship.

Finally, thank you to my parents for their constant support and love. They have always allowed us to believe that we can do anything we want, and have provided us with every opportunity to succeed. Thank you to my brother, Jeffrey, and my sisters, Courtney and Julie. Their unconditional love and support has been wonderful. It's amazing watching you grow into magnificent people, and I know your potential is unlimited. And of course, thank you to my best friend and fiancé, Adam. You have always been there for me, no matter what. Knowing I can escape home with you and the two sets of stinkin twinks makes everything worth it. I love you.

TABLE OF CONTENTS

LIST OF TABLES

LIST OF FIGURES

CHAPTER I

INTRODUCTION

Hepatic fibrosis is a disease that is caused by incessant irritation of the liver tissue, and results in the formation of scar tissue, which impairs liver function. Fibrosis of the liver is a progressive disease that, if diagnosed in early stages, has potential to be nearly reversible, whereas progression into later stages of fibrosis leads to effects that are not easily treatable and can be life-threatening. If left untreated, fibrosis can progress to cirrhosis, which lead to over 28,000 deaths in the United States in 2003 [1]. Current treatment for fibrosis is limited. The underlying injurious process in fibrosis is most often chronic alcohol ingestion, chronic viral hepatitis, non-alcoholic steatohepatitis (NASH), or immune-mediated liver injury [2, 3]. The primary concern in treatment is removal of the injurious agent, which can halt progression of the disease. However, the elimination of the scar tissue is limited if the only treatment is removal of the affecter, and thus the only curative treatment is liver transplantation [2]. It has been identified that fibrosis is a bidirectional process, so that a reverse procedure could be elicited that causes removal of the scar tissue, allowing the liver to heal and eliminating the need to liver transplantation. For this reason, research has been focused on identifying the molecular mechanisms of fibrosis to elicit production of an antifibrotic treatment. As new molecular therapies are developed, the effectiveness needs to be assessed. The current gold standard for liver fibrosis diagnosis and grading is liver biopsy, which is an invasive, and often painful, procedure. In addition, liver biopsy has demonstrated poor reproducibility. To prevent repetitive liver biopsies, researchers have been focused on developing non-invasive diagnostic techniques.

In a variety of cases, research has identified a deviation from baseline norm in the material properties of diseased tissue. An example of such a material property is the elastic modulus, or Young's Modulus, which quantitatively describes the stiffness of a tissue. For example, many types of cancer are significantly stiffer than the normal tissue. This is also the case in fibrosis; the liver becomes progressively stiffer as the disease progresses due to changes in the extracellular matrix (ECM) mainly due to increased amounts of collagen. The change in material properties associated with disease progression is being utilized as a non-invasive diagnostic measure in such techniques as ultrasound elastography (USE) and magnetic resonance elastography (MRE), which evaluate the stiffness of the liver. However, to fully utilize these techniques as a diagnostic tool, it is necessary to understand the underlying physical progression of the disease, and how this correlates to the modulus of the liver.

The goal of this research was to develop a unique evaluation system that would link histological analysis of fibrosis to mechanical analysis of the liver. Ideally, the evaluation system would be adaptable to a variety of situations and would transcend a multitude of imaging techniques to allow a variety of applications. In addition, the analysis would not only provide mechanical evaluation of the liver, but also histological analysis of the fibrosis state, to allow insight to the relationship between the progression of fibrosis and the modulus of the liver.

CHAPTER II

MECHANICAL TESTING ASSAY FOR FIBROTIC MURINE LIVER

Abstract

Hepatic fibrosis is a progressive disease in which progression is correlated to liver mechanical properties. This correlation may be used to assess the state of the disease, and hence methods to determine the elastic modulus of the liver are of considerable interest. In order to assess the diseased state of the liver accurately, controlled experiments to establish baseline modulus values for healthy livers as well as diseased livers must be conducted. In this paper, a protocol for mechanical testing combined with finite element modeling is presented that allows for the evaluation of normal and fibrotic murine livers using multiple testing methods. The protocol employs a portion of liver tissue suspended in a cylindrical gel for CT imaging and mechanical testing. A finite element model is built from the CT images, and boundary conditions are imposed in order to simulate the testing conditions of the gels. The resulting model surface stress is compared to that obtained during mechanical testing which subsequently allows for direct evaluation of the liver modulus. This system was used to study five fibrotic livers, three control livers, and three normal livers. Though the sample sizes were small, the preliminary results indicate that the livers could be identified within the gel, and the fibrotic livers could be identified as having a higher modulus than the control livers. In addition, a separate mechanical indentation test and histological analysis were performed on the livers for comparisons and analysis. The moduli evaluations for non-diseased livers were estimated as 0.62 +/- 0.09 kPa, and 0.59+/- 0.09 kPa for indenter and model-analysis tests, respectively. Moduli estimates for diseased liver ranged from 0.85-1.64 kPa and 1.42-1.88 kPa for indenter and model-

analysis tests, respectively. The model-calculated modulus was well correlated to the indenter modulus, excluding one presumed outlier. The results also showed a clear difference between non-diseased and diseased livers with qualitative agreement between disease scores and mechanical properties. Further testing with a larger sample size is necessary to corroborate these initial results, but the preliminary implication is that the developed gel-tissue assay system could be utilized for controlled evaluation of soft-tissue moduli.

Introduction

Several types of pathological changes within soft tissue disease are correlated to changes in mechanical properties. For example, clinical examinations as well as direct mechanical testing have indicated that disease conditions can result in changes in the elastic modulus of the tissue. Furthermore, the pathological change in tissue elasticity has become the basis for palpation as a diagnostic tool. Advances in medical imaging have allowed for the measurement of tissue displacement or deformation which can be directly related to the tissue elasticity, thus allowing evaluation of changes in the state for many different biological tissues. However, in order to interpret a change in elasticity, an understanding of normal baseline elasticity conditions must be established as well as a systematic understanding of changes in elasticity with disease progression and their relationship to histological variations. Towards this end we have investigated the elastic moduli of murine livers under various controlled conditions.

Research has been performed extensively evaluating the elastic modulus of many biological tissues including skin, breast, prostrate, brain, spleen, and muscle, among others [4-8]. One potentially important area of investigation is the mechanical properties of progressive changes in liver with fibrosis. Hepatic fibrosis is a progressive disease that increases the elastic modulus of the liver due to changes in composition.

Potentially this disease could be monitored by assessing the tissue elastic modulus [9, 10]. Recent indications are that fibrosis may be reversible with proper treatment, but, as is the case for many diseases, early diagnosis is required for the best clinical outcome [2, 3]. Approaches have been developed that evaluate the modulus of the liver, through such methods as ultrasound elastography (USE) and magnetic resonance elastography (MRE) [11-14]. While these methods are of potential value, there is a sparse basis for correlating elasticity changes, disease progression, and histological analysis.

Previous research characterizing liver mechanical behavior has been performed, usually with the intent to identify liver modulus under specific imposed conditions that correlate to conditions experienced during particular evaluation techniques. One goal of this paper is to devise a more comprehensive mechanical evaluation system that could be utilized for an array of applications. The motivation for determining liver moduli is generally divided into two categories. The first concerns the evaluation of liver modulus for confirmation of elastography techniques within a realistic system [14-17]. The second seeks to generate a reasonable evaluation of liver modulus for software-based surgical simulation [18-21]. It is important to note that among these applications, variable loading environments exist and must be taken into account when determining properties. For example, in MRE, low frequency (50-200Hz) shear waves are propagated into the tissue of interest and displacement measurements are recorded. This type of excitation would reflect rapid strain rates as opposed to the quasi-static loading associated with surgical manipulation or traditional ultrasound elastography. The literature supports varying stress-to-strain behavior at different loading rates [22-24] for soft tissue. For example, in brain tissue, Donnelly et al. [22] measured stresses for equivalent strains that were 4-5 times higher with loading rates akin to 45 Hz. Krouskop et al. examined breast and prostate tissues and found increases in mechanical properties when testing over frequencies from 0.1-4 Hz [23]. Kiss et al. determined

viscoelastic models that captured canine liver mechanical tests at a range of frequencies (0.1-400 Hz) and also saw the trend of increasing stiffness with frequency [24]. While these tests are difficult to conduct, it is important to realize that more work is necessary which connects changes in mechanical properties to the cytoarchitectural changes in tissue associated with different disease states. Without understanding the relationship between structure and function change, the utility of elasticity imaging methods will be difficult to demonstrate.

This paper presents a novel ex-vivo gel-assay system that combines mechanical testing, imaging, and finite element modeling to monitor the changes in mechanical properties of a murine liver fibrosis model. To qualify our results, separate indentation testing was performed and compared to that of the gel-assay technique. While many previous studies have been predominantly concerned with human or large animal evaluations, this protocol is focused on small animal models.. The obvious advantage of targeting small animal applications is that it allows for rapid evaluation of many subjects, multi-modal image registration (magnetic resonance, computed tomographic, positron emission tomography, bioluminescence, etc.), access to numerous disease models, and the ability to test pharmacological therapeutics within these systems. The ultimate goal of this testing protocol is to provide a controlled experimental platform to begin to correlate structural changes in soft tissue with the concurrent changes induced by disease. We evaluated the feasibility of this protocol in a limited sample size (n=5 fibrotic livers, n=2 control livers for gel-assay, n=3 control livers for indentation, n=3 normal livers with no intraperitoneal injections). The findings indicate consistency between histological disease scoring and the gel-assay system. The separate indentation tests were consistent with the gel-assay results for control and normal livers. While stiffening of the tissue was measured by both gel-tissue assay and indentation tests, there was inconsistency among the absolute values established for fibrotic livers.

It did appear that the offset between the values among the two testing methods may be correlated. With respect to histological grading, a relationship between disease score and indentation test did not appear to be present; however, an observational trend is suggested between gel-tissue assay and disease grade.

Methods

The protocol used to evaluate fibrotic and non-diseased murine livers involves a series of steps as shown in Figure 1. This three-pronged investigation sought to characterize liver tissue in three distinct ways: (1) mechanical testing with an ex vivo gel-tissue assay, (2) mechanical testing by indentation, and (3) tissue characterization via histochemical staining.

Fibrosis Model and Disease Scoring

Adult C57 mice (18-20 g, 8-10 weeks of age) purchased from Jackson Laboratory were housed in cages with a 12-hour light/dark cycle (6 a.m. to 6 p.m.) and provided with rodent chow and tap water ad libitum. All animals received humane care in compliance with the institution's guidelines, and animal procedures were approved by the Institutional Animal Care and Use Committee, which is certified by the American Association for Accreditation of Laboratory Animal Care. The animals were divided into three groups. The first group of mice consisted of five animals that received weekly intraperitoneal (IP) injections of carbon tetrachloride (Sigma Chemical, St. Louis, MO) mixed with olive oil (Sigma Chemical, St. Louis, MO) in a 1:4 ratio, respectively. Each dose of CCl_4 was 1 ml/kg per injection. The second group of mice consisted of three animals and was the control group. This group received weekly IP injections of pure olive oil. The third group consisted of three animals and did not receive IP injections (of note these mice were several weeks older than groups 1 and 2). One mouse from the

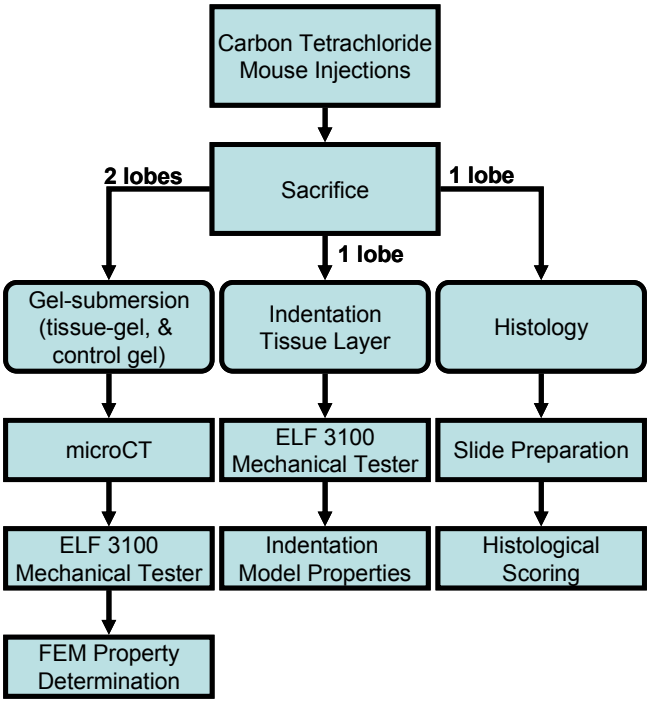

Figure 1. General mechanical testing framework for murine liver system.

fibrosis group was sacrificed weekly, starting five weeks after the first injection. A control mouse was sacrificed on weeks five, six, and eight. The liver was removed and divided into three sections. The first, and largest, section consisted of two of the four lobes, and was embedded in the polyacrylamide gel. The third lobe was preserved for use in indenter testing, and the fourth lobe was frozen for future analysis. The liver lobe that was designated for indenter testing was also utilized in histological analysis. After indenter testing, the tissue was fixed in 10% buffered formalin, dehydrated in graded ethylic alcohol, and embedded in paraffin. Sections were generated with a thickness of 5 micrometers and were stained with hematoxylin/eosin (H/E) or 0.1% Sirius red. The H/E stained sections were analyzed under light microscope for histopathological assessment. The Sirius red stained sections were used for fibrosis evaluation. These specimen were scored using Ishak (score 0-6) systems, which is commonly used in clinical pathology. Mild fibrosis was defined as Ishak 0-1, advanced fibrosis as Ishak 2-4 and cirrhosis as Ishak 5-6 [25].

Gel-Tissue Assay Construction

In order to provide a controllable evaluation technique, a system of embedding extracted murine livers in a cylindrical gel has been developed. This gel-matrix provides a reference material for evaluation, provides a measurable contrast in elasticity between the gel and liver, and allows for use of true organ shape by building a model based on microCT scans of the gel. In addition, the cylindrical gel could easily be utilized in multiple imaging modalities. Given that the gel modulus is being used as the elastic reference for liver property assessment, the gel selection is of considerable importance. Two materials are commonly mentioned in literature as being utilized for phantom generation and submersion techniques: agarose (Research Products International Corp, Mt. Prospect, IL) and polyacrylamide (BioRad Laboratories, Hercules, CA). Our work

required two key characteristics of the gel utilized for liver submersion: (1) the gel modulus must be variable and relatively simple to control, and (2) gel properties needed to be relatively static over time, i.e. thermal shifts needed to be minimized, and viscoelastic effects need to subside quickly.

Tests were performed in order to assess both the constituent percentage to modulus relationship and the time dependence of the modulus values. Both agarose and polyacrylamide materials have the advantage that the stiffness of the gel can be modified by altering the percentage (by weight) of agarose or polyacrylamide in the gel. For the agarose samples, eight gels were generated, with agarose percentages of 0.3, 0.4, 0.5, 0.6, 0.75, 1.0 and 1.25. In the polyacrylamide case, six gel samples were tested, ranging from 3 to 6 percent polyacrylamide in 0.5 percent increments. All gels were created in Petri dishes that measured 10 cm in diameter and 1.1 cm deep. The testing protocol consisted of the application of a 5 percent precompression. Step compressions were applied in 0.5 percent increments for a total of 5 percent additional strain, with a 60 second dwell after each compression. The force values were collected at the end of each dwell period, and were utilized with the corresponding compression values to generate stress and strain data for the gels. A linear regression was performed on the stress-strain data to approximate the modulus for each gel sample. The same material testing protocol was implemented to assess the thermal-dependence of the gel moduli. Two samples were manufactured for each gel type; the percentage of agarose or polyacrylamide was chosen based on the modulus evaluation results. The gels were tested immediately after generation, and then at each subsequent hour for four hours. The modulus values for the samples were calculated as previously described.

In addition to stable gel properties, the gel-tissue samples also needed to be appropriately shaped for both imaging applications and material testing. Ideally, this

meant a small sample size with a uniform shape. To achieve this, the gel samples were generated in Petri dishes that had a known diameter. This created a cylindrical shape with a flat top and bottom surface that were parallel, a measurable surface area, and a consistent height. The process of tissue submersion involved a simultaneous resection of the liver and the mixing of the base components of the polyacrylamide gel. The components were 1 molar Tris buffer, deionized water, and ammonium persulfate (APS). Graphite flakes (Sigma-Aldrich Chemie GmbH, Buchs, Switzerland) were also added to the base solution; these were necessary to provide ultrasound contrast (although this will not be reported in this work at this time) for imaging. During liver resection, the buffer solution was mixed as indicated in Table 1. Once the liver was removed and sectioned, the portion dedicated to the gel sample was weighed using a digital balance. In order to generate the individual gel sample, the buffer solution and acrylamide/polyacrylamide were mixed in a Petri dish according to the proportions indicated in Table 1. To provide a perceivable distinction between the liver and gel in the CT scans for segmentation purposes, a computed tomography (CT) contrast agent, Optiray (Mallinckrodt Inc, Hazelwood, MO), was included in the gel mixture. The liver sample was then suspended in the liquid gel using forceps, and TEMED was added, which initiates the polymerization reaction to cause solidification of the gel. The solution was agitated during the solidification process, which required approximately two minutes, using a small pipette; the agitation prevented settling of the graphite flakes. This process was performed for the fibrosis livers, the control livers, and the normal livers; gels with a fibrotic liver embedded are referred to as *fibrosis gels*, gels with a control liver embedded are referred to as *control gels,* and gel with a normal liver embedded are *normal gels*. In addition, a *reference gel* was generated, which was produced as described above, without the addition of the liver sample. This *reference gel* was utilized in material testing in order to evaluate the modulus of the polyacrylamide gel generated on the

Table 1. Polyacrylamide Gel Recipe

Polyacrylamide Gel Recipe		
Buffer Solution		***Individual Gel Recipe (5% Polyacrylamide)***
38.2 mL deionized H_2O		6.67 mL buffer solution
1.3 mL 1 M Tris buffer		1.33 mL 30% Acrylamide/Polyacrylamide
0.5 mL 10% APS solution		0.2 mL Optiray CT contrast
1.5 g graphite		0.07 mL TEMED

occasion of each fibrotic liver evaluation. Five fibosis gels, three control gels, and three normal gels were generated over the course of the research, with seven corresponding reference gels (the normal gels were generated in two groups, with two reference gels, after the initial evaluation of the fibrosis and control gels).

Imaging

After the gel had congealed, microCT scans were obtained using the Imtek microCAT II scanner (Concord/CTI, Knoxville, TN). The resolution of the microCT image voxel was 115 X 115 X 115 microns. These scans were later utilized for finite element model generation. The gel sample was placed on the scanner bed and made level by adjusting its positioning based on prescan information from the scanner. The images were also later leveled using image registration features in the image segmentation software. CT scans were obtained for fibrosis, control, and normal gels, but not for the reference gels. After scanning, the gels were transferred to the material testing lab and immediately tested. The total time between sacrifice and testing ranged from 1 – 2 hours.

Indenter & Traditional Compressive Material Testing

Individual liver lobes obtained during resection of the liver were placed in 0.9% NaCl and refrigerated until testing could be performed, which was less than one hour. Indenter tests were performed on the liver lobes in order to acquire an elasticity value to which results from the gel-tissue assay could be compared. All material testing was performed utilizing the Enduratec Electroforce 3100 tester (Bose, Enduratec Systems Group, Eden Prairie, Minnesota). The material tester setup is shown in Figure 2. A 50-g transducer (Honeywell Sensotec, Columbus, Ohio) was attached to the upper arm of the tester, the indenter tip was attached to the transducer using a coupling device

manufactured for this purpose, and the tip was lubricated with non-stick oil-based lubricant spray. The testing configuration is shown in Figure 3. The indenter tip used in all tests was a spherical tip with a radius of 1.5 mm. A spherical tip was chosen in order to minimize damage to the tissue so that the liver lobes could subsequently be utilized for histological testing. The liver lobes were placed on the lower platen of the material tester, and the force and displacement values were zeroed prior to lowering the indenter. The indenter tip was manually lowered until it made contact with the liver surface, which was determined by visual inspection and by observation of a sudden increase in the force values registered by the transducer. Contact between the liver and indenter was regulated between specimens by maintaining a force value between 0.01 and 0.03 g at initial contact. The liver lobe was situated on the platen relative to the indenter so as to provide a uniform surface for indentation. The indentation occurred at the thickest portion of the liver, in an area where there were no steep surface gradients.

Development of an indentation protocol that correlated to the compression protocol was necessary in order to generate results that could be analyzed relative to one another. However, in indentation testing, it is necessary that the depth of indentation not exceed the radius of the indenter tip, in order to prevent aberrant behavior of the tissue indentation model. In order to remain within the confines of the indenter system, the indentation protocol consisted of three compressions to a depth of 0.4 mm. The compressions were applied at a rate of 0.4 mm/s, which provides a quick application of strain. Each compression was held for a 60 second dwell period, and then released again at a rate of 0.4 mm/s. The indenter returned to zero position, and remained there for 60 seconds, at which point another compression occurred in the same manner. Each liver was measured after testing using a digital caliper to determine the thickness of the specimen at the region of indentation.

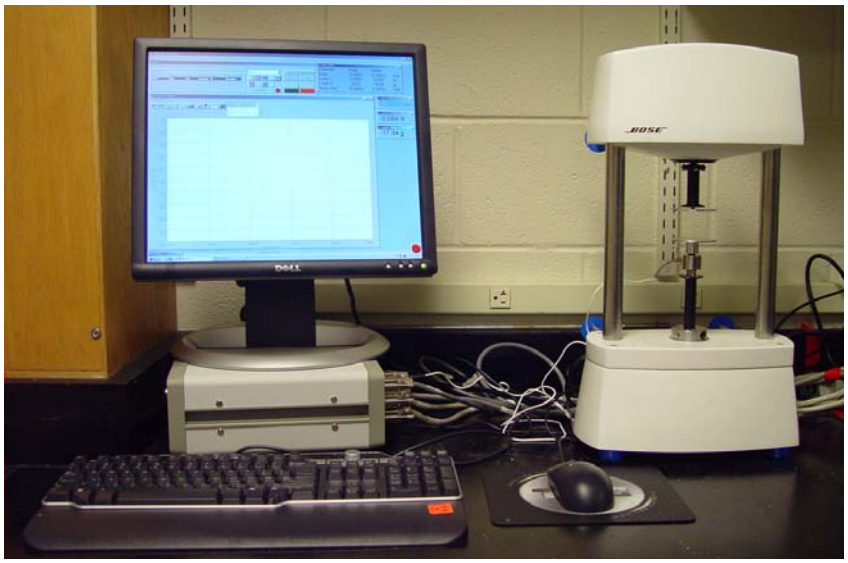

Figure 2. Material testing setup used for gel and liver testing.

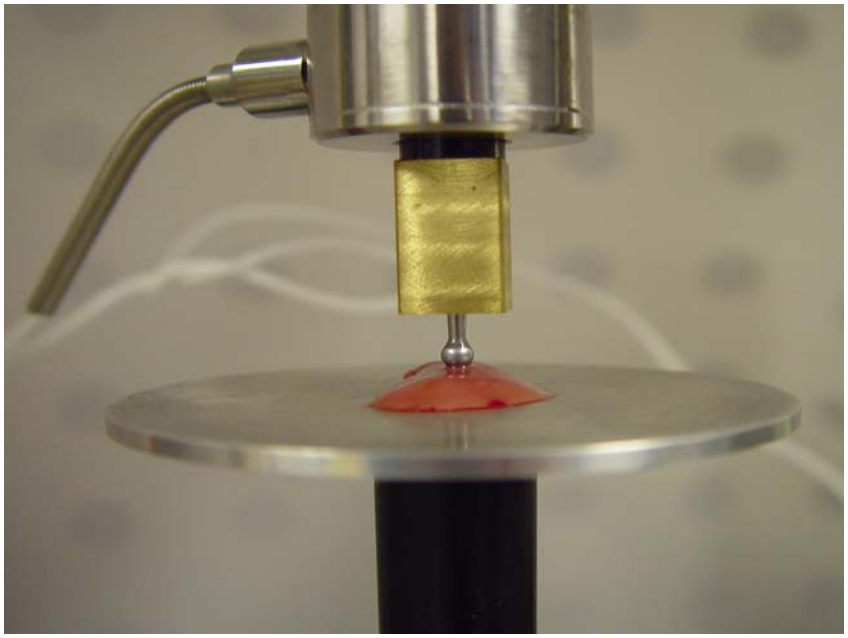

Figure 3. Close up of liver indentation setup. The liver was positioned so that contact with the indenter occurred at a point where the liver was uniform in height

The gel-tissue cylindrical specimen was tested using traditional compression. For this work, the Enduratec ELF 3100 testing system (Bose, Eden Prairie, Minnesota) was utilized. Due to the increased size of the specimen, the load cell used was a 250 gram transducer (Honeywell Sensotec, Columbus, Ohio). Figure 4 illustrates the setup for compression testing. Each gel was weighed using an analytical balance and measured using digital calipers (diameter and height) prior to testing. Both surfaces of the gel were lubricated, again using the non-stick oil-based lubricant spray. The material tester was zeroed after placing the gel specimen on the platen, so that the weight of the gel was not considered in the measured force. The platen was then lowered until initial contact with the gel surface. This was determined by visual cues as well as a negligible increase in the force reading. For the compression case, the initial force values were limited to between 1 and 2 grams. A precompression of 0.3 mm was applied to each gel prior to testing in order to ensure full contact with the gel surface. The testing protocol consisted of a series of step compressions, applied in 0.05 mm increments, from 0.35 mm to 0.65 mm. After each step, the compression dwelled for 60 seconds to allow the force to reach steady state. The test was performed twice for each gel.

Computational Model for Indentation and Gel-Tissue Assay

With respect to the indentation testing data, the mechanical properties were determined using the model suggested by Stevanocić et al. which modeled the contact between a rigid sphere and an elastic layer bonded to a rigid substrate [26]. The assumption is that the boundary defined between the liver and the bottom platen experiences no-slip conditions, and hence the liver can be considered an elastic medium bonded to the rigid platen. The equation derived by Stevanocić et al is:

Figure 4. Gel compression testing setup.

$$\frac{\mathbf{a}}{\mathbf{a_L}} = \mathbf{1} - \mathbf{c_3}\,\mathbf{exp}\left[\mathbf{c_1}\left(\frac{\mathbf{t}}{\mathbf{a}}\right)^{\mathbf{c_2}}\right] \tag{1}$$

where c_1, c_2, and c_3 are correlation coefficients, which, based on the analysis by Stevanocić et al, are defined as -1.73, 0.734, and 1.04, respectively, **a** represents the contact radius, $\mathbf{a_L}$ is the contact radius corresponding to an infinitely thick elastic layer, and **t** is the layer thickness. The contact radius, **a**, for a spherical indenter can be calculated from:

$$\mathbf{a} = \sqrt{2\rho\mathbf{d}} \tag{2}$$

where **ρ** is the radius of the spherical indenter tip and **d** is the penetration depth of the indenter. To calculate the contact radius for an infinitely thick elastic layer (a_L) , the Hertz relation must be consulted:

$$\mathbf{a_L} = \left[\frac{\mathbf{3}}{\mathbf{4}}\frac{\mathbf{(1-\nu^2)}}{\mathbf{E}}\mathbf{F}\rho\right]^{\mathbf{1/3}} \tag{3}$$

where **E** denotes the elastic modulus of the medium, **v** the Poisson's ratio, and **F** the applied load. For this research, if a Poisson's ratio of 0.45 is assumed for tissue, all of the elements of equation 3 are known except for Young's Modulus of the tissue. Substituting equations 2 and 3 into equation 1 and solving for the modulus gives the equation utilized for modulus calculation:

$$\mathbf{E} = \frac{\mathbf{3}}{\mathbf{4}}\mathbf{(1-\nu^2)}\mathbf{F}\rho\,\frac{\left\{\mathbf{1} - \mathbf{c_3}\,\mathbf{exp}\left[\mathbf{c_1}\left(\frac{\mathbf{t}}{\mathbf{a}}\right)^{\mathbf{c_2}}\right]\right\}^{\mathbf{3}}}{\mathbf{(2\rho d)^{\frac{3}{2}}}} \tag{4}$$

The modulus for each liver lobe was calculated for each of the three indentations. The indentation depth was taken as the average indentation over the course of the 60 second dwell, and the applied force utilized was the average force over the last 20 sampling points of the dwell, at which time the response curve had become relatively

constant. The three calculated modulus values were then averaged to obtain the final elastic modulus value for each liver.

For the traditional compression test, a more complex model analysis was performed. A critical component in this analysis was the selection of the model to represent the continuum of interest. In this work we have chosen a Hookean elastic solid. This model assumes a symmetric, isotropic, specimen in equilibrium under small strains. These assumptions linearize the strain tensor and simplify Cauchy's law from 36 stiffness constants to 2 (Young's modulus E, and Poisson's ratio λ) and use the traditional mechanical equilibrium equation. For this work, we have determined that a Poisson's ratio of 0.45 for our gel and tissue has performed reasonably well. This value would correlate with a 9:1 ratio of the Lamé constants (λ:G with G the shear modulus, and λ) which is reasonably below the convention for Poisson locking (sometimes called mesh locking and typically has λ»G, or v→0.5). In past work, we have found for general soft tissue organs that 0.45 has captured 1st order elasticity effects for liver and brain reasonably well [27-30].

The set of mathematical equations governing linear elastic deformations for this model is written:

$$\nabla \bullet \mathbf{G}\nabla\vec{\mathbf{u}} + \nabla\frac{\mathbf{G}}{\mathbf{1}-\mathbf{2}\nu}\left(\nabla \bullet \vec{\mathbf{u}}\right) = \mathbf{0} \tag{5}$$

where $\mathbf{G} = \mathbf{E}/\mathbf{2(1+\nu)}$ is the shear modulus, **E** is Young's Modulus, **v** is Poisson's ratio, and $\vec{\mathbf{u}}$ is the vector of Cartesian displacements. Given (5), a numerical solution to the coupled set of linear partial differential equations is performed using a weighted residual method. The method begins with standard residual weighting, and integration shown here in (6),

$$\left\langle G\nabla\vec{u}\bullet\nabla\phi_i\right\rangle+\left\langle\frac{G}{1-2\nu}(\nabla\bullet\vec{u})\nabla\phi_i\right\rangle=\iint\tilde{\sigma}_s\bullet\vec{n}\phi_i dS \tag{6}$$

where an integration by parts has taken place which reduces the basis function order requirement, and introduces the surface integral via the divergence theorem. In (6), the $\langle\bullet\rangle$ operator indicates integration over the problem domain, and ϕ_i is the i^{th} member of a complete set of scalar functions of position, in particular, the standard C^o local Lagrange polynomial interpolants associated with finite elements. In true Galerkin fashion, the unknown displacement vector is also expanded using a Lagrange basis function of position as shown in (7),

$$u(x,y,z)\approx\hat{u}(x,y,z)=\sum_{j=1}^{4}u_j\phi_j(x,y,z) \tag{7}$$

The element used in this work was the standard linear tetrahedral element. Upon substituting the basis function, the local weighted residual expression for the i^{th} equation and the j^{th} set of displacement coefficients can be written as,

$$[K_{ij}]\{\vec{u}_j\}=\{\vec{b}_i\} \tag{8}$$

where

$$[K_{ij}]=\begin{bmatrix}G\left\langle\frac{2(1-\nu)}{1-2\nu}\delta_{xx}+\delta_{yy}+\delta_{zz}\right\rangle & G\left\langle\frac{2\nu}{1-2\nu}\delta_{yx}+\delta_{xy}\right\rangle & G\left\langle\frac{2\nu}{1-2\nu}\delta_{zx}+\delta_{xz}\right\rangle\\ G\left\langle\frac{2\nu}{1-2\nu}\delta_{xy}+\delta_{yx}\right\rangle & G\left\langle\delta_{xx}+\frac{2(1-\nu)}{1-2\nu}\delta_{yy}+\delta_{zz}\right\rangle & G\left\langle\frac{2\nu}{1-2\nu}\delta_{zy}+\delta_{yz}\right\rangle\\ G\left\langle\frac{2\nu}{1-2\nu}\delta_{xz}+\delta_{zx}\right\rangle & G\left\langle\frac{2\nu}{1-2\nu}\delta_{yz}+\delta_{zy}\right\rangle & G\left\langle\delta_{xx}+\delta_{yy}+\frac{2(1-\nu)}{1-2\nu}\delta_{zz}\right\rangle\end{bmatrix},\{\vec{u}_j\}=\begin{Bmatrix}u_j\\v_j\\w_j\end{Bmatrix},$$

$$\{b_i\}=\begin{Bmatrix}\vec{x}\bullet\oint\sigma\bullet\vec{n}\phi_i ds\\ \vec{y}\bullet\oint\sigma\bullet\vec{n}\phi_i ds\\ \vec{z}\bullet\oint\sigma\bullet\vec{n}\phi_i ds\end{Bmatrix} \tag{9}$$

and $\delta_{kl} = \frac{\partial \phi_j}{\partial k} \frac{\partial \phi_i}{\partial l}$. With (8), the contribution from each tetrahedral element can be determined, and a global stiffness matrix can be constructed. An iterative matrix solver was used to solve the sparse system which used a biconjugate gradient solver with an incomplete LU preconditioner [31]. To construct the domain, microCT image volumes were acquired prior to compression. In all experiments, the control, fibrosis, and normal gel systems were imaged and the gel and tissue were segmented using AnalyzeAVW [Mayo Foundation for Medical Education and Research, Rochester, MN]. Due to the doping of the gel with CT contrast, it was relatively simple to extract the liver volume using the standard morphometric operations of threshholding and region-growing. The segmented volumes were found to agree with estimated volumes based on an assumed liver tissue density and the measured mass of the tissue. Upon completion of the segmentation, a marching cubes surface description was generated and used as a bounding description for a custom-built tetrahedral mesh generator [32]. Figure 5 illustrates the geometric model construction process with Figure 5a demonstrating a representative CT slice of the murine liver within a contrast-doped gel. Figure 5b illustrates a homogeneous gel tetrahedral mesh (as can be seen, small gel surface defects were even captured with the process). Figure 5c illustrates the extracted liver tetrahedral mesh within the gel system.

The boundary conditions reflected an unconfined compression that prescribed a fixed normal displacement (Dirichlet) on the majority of the top surface, but was allowed to slip laterally (Neumann). This was achieved experimentally by placing a lubricant on the contact surfaces. More formally, the boundary conditions on the majority of the top surface were,

$$u_n = -d, \sigma_{t1} = 0, \sigma_{t2} = 0 \tag{10}$$

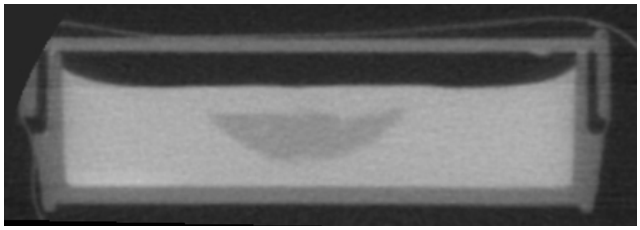

a

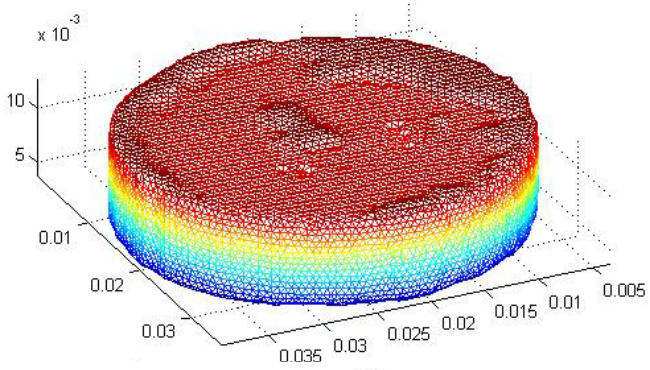

b

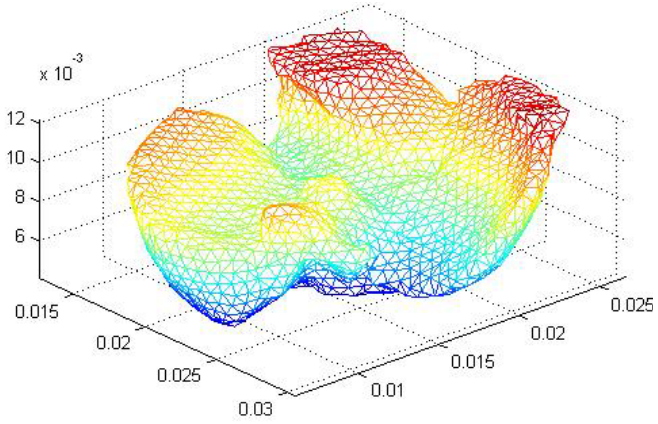

c

Figure 5. Computational domain construction with (a) liver microCT, (b) gel tetrahedral mesh, and (c) liver tetrahedral mesh extracted from gel/liver model.

where **d** is the fixed compressive displacement magnitude. Similarly, at the bottom surface, the boundary conditions were,

$$u_n = 0, \sigma_{t1} = 0, \sigma_{t2} = 0 \tag{11}$$

In order to ensure solution uniqueness, at least one Dirichlet condition is required in the lateral directions. To achieve this, nodes on the top and bottom surface that were within approximately 30 microns of the center-line were fixed on each surface to restrain their movement laterally. The remaining boundary conditions for the sides of the gel were stress-free, i.e.

$$\sigma_n = 0, \sigma_{t1} = 0, \sigma_{t2} = 0 \tag{12}.$$

The goal of this work is to determine by multiple methods the mechanical properties of normal and diseased mouse livers as altered by chemically-induced fibrosis. More specifically, this paper serves to compare modulus estimates as provided by a novel model-based gel-tissue assay and that provided by indentation theory. In the model-based comparison method, the above model is compressed in simulation to a degree that matches the physical compression of its mechanically tested physical counterpart. For each mouse liver-gel, a corresponding homogeneous gel is also constructed. From the mechanical tester, an average force applied to either gel surface (homogeneous or liver-gel system) is recorded. By measuring the contact surface area, an average stress can consequently be determined. Similarly, in our simulation, a compression is prescribed according to (10), (11), and (12). Once the boundary conditions are prescribed, a solution is calculated which is based on an initial estimate of the gel and liver properties for each of the gel systems (homogeneous and liver-gel systems). Once the displacement solution is calculated, the unused Galerkin equations associated with implementing Dirichlet conditions along the compressing surface can be used to estimate the boundary integral associated with the weighted residual form, i.e.

$$\iint \tilde{\sigma}_s \bullet \vec{n}\phi_i dS = \sum_j \vec{u}_j \left\langle G\nabla\phi_j \bullet \nabla\phi_i \right\rangle + \sum_j \vec{u}_j \left\langle \nabla\phi_j \frac{G}{1-2\nu} \nabla\phi_i \right\rangle \quad (13).$$

Once the right-hand-side of equation (9) is constructed, the left-hand-side surface integral can be solved for the local normal stress distribution which can subsequently be averaged and compared to the respective mechanically-tested value. The process involves fitting the homogeneous gel modulus first. Once determined, this is the assumed property of the gel within the heterogeneous liver-gel system. The properties of the liver are then determined by the same process of comparing measured to predictive average stresses.

Results

The initial gel testing for the comparison between agarose and polyacrylamide gel proved deterministic in the gel selection. Both gels were able to be controlled for modulus based on the percentage of agarose or polyacrylamide, and could be adapted to generate the desired modulus (5-7 kPa). The desired modulus value was achieved with 0.5% agarose and with 5% polyacrylamide, so both were effective in this regard. However, we found that agarose is very sensitive to thermal effects. In our investigation, the modulus of the agarose samples decreased by 15.5% over the first hour and 44.8% over the full four hours. Polyacrylamide did not demonstrate the same extremity of thermal effects as agarose. The polyacrylamide samples demonstrated a decrease in modulus of only 4.8% in the first hour, and a total of 12.6% over the four hours of experimentation. Based on these findings, polyacrylamide was chosen as the background gel. Figure 6 illustrates the average stress-strain behavior of the reference gels with the values extracted after the 60 second dwell period. Generating an estimate of the reference gel properties was important to the model-based characterization of mouse-liver properties. Given that gel-tissue system and reference gel were made at

the same time, the reference gel became essential for fitting the properties of the liver in the gel-tissue system. Figure 7 illustrates a similar stress-vs-strain application for a gel containing a murine liver, with data points again collected after the 60 second dwell. Figure 8 illustrates the excitation and dwell period of a typical indentation test.

The results from the indentation testing of the liver lobes are given in Tables 2 and 3. Table 2 contains the data for the fibrotic livers. The values are given as the average of the three indentation tests for each liver. Table 3 contains the data for the control livers and the normal livers without treatment. The average value and standard deviation are given for the three controls, the three normals, and the non-diseased group, which contains all six control and normal livers. In each case, the standard deviation is small, indicating the variability of inter-sample moduli (although this must be tempered with the realization that the sample size is quite modest in this report). The model-based calculation of fibrosis, control, and normal liver moduli are given in Tables 2 & 3 also. For the model-based simulations, the control liver from 6 weeks of injections (liver 2) was not available so model data from only two control livers were used to determine the control liver properties. In both the model-based and indenter cases, the control and normal moduli did not vary over the course of the experimentation. When considering the control/normal liver moduli as compared to the fibrosis liver moduli, both the indenter testing and the model results show a marked difference between groups.

The only occasion where the fibrosis liver does not have a modulus that is significantly higher than the control/normal livers is the indenter test for liver 5, where the modulus was less than 1 kPa. The model evaluation resulted in a modulus of over 1.4 kPa, which is more than twice the average non-diseased value. There does seem to be a general trend in that the model fibrosis evaluation resulted in moduli that were higher than the indenter moduli.

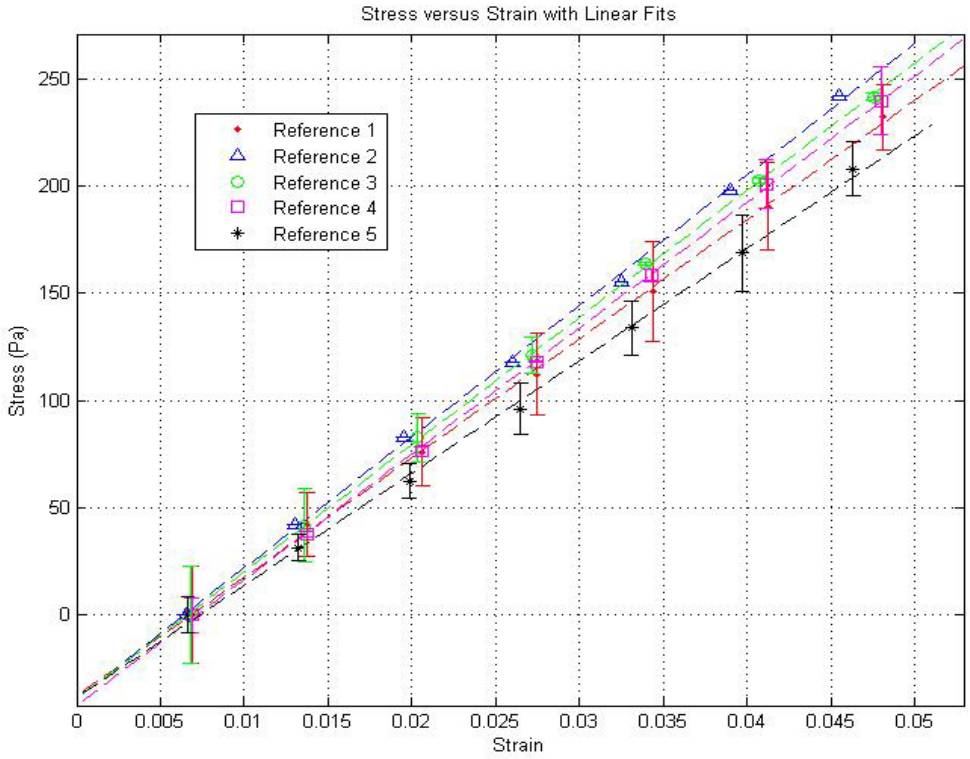

Figure 6. Stress-strain curves for reference gels from compression testing. A precompression of approximately 4% strain (0.3 mm) was applied prior to testing. The values are average values for the two compression tests performed on each gel, with error bars indicating the standard deviation of the two tests.

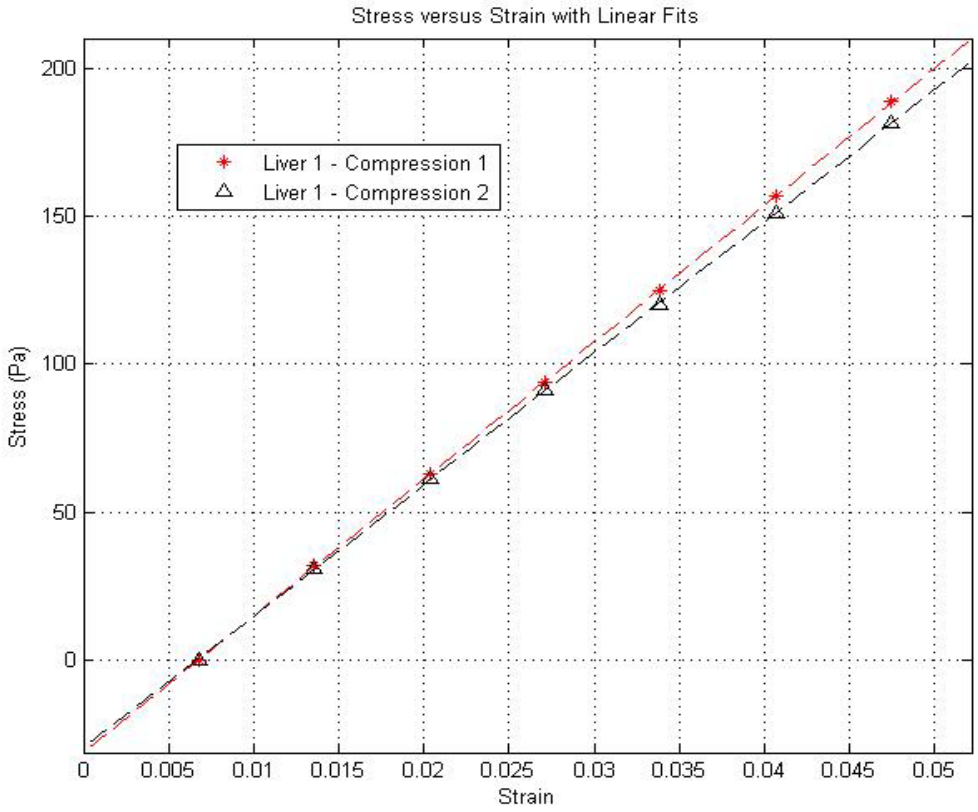

Figure 7. Stress-vs-strain behavior taken after the 60 second dwell for the gel-tissue system of a fibrotic specimen. The two curves represent the two compression tests.

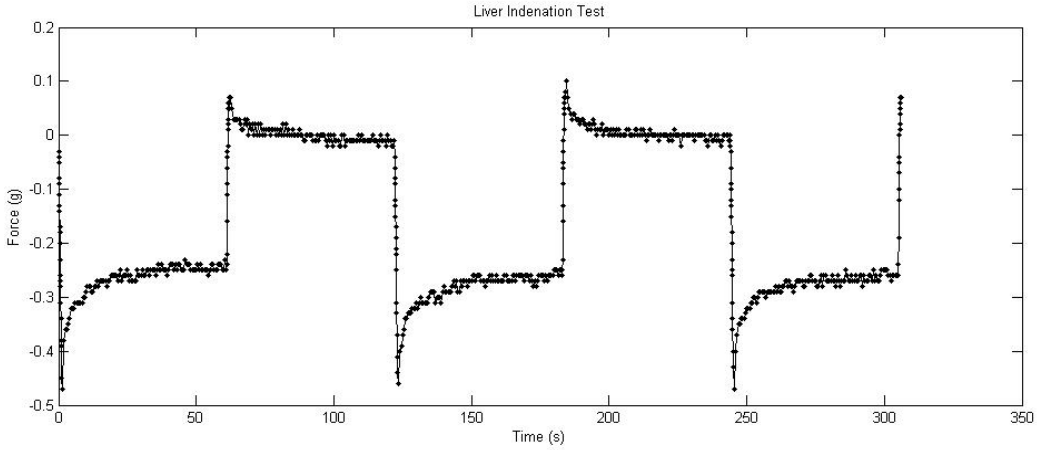

Figure 8. Example of force data obtained from liver indentation test. The temporal decay of the force data during sustained compression indicates the viscoelastic nature of the tissue. However, the effect dampens and a steady state has been approximately established at the end of the dwell.

Table 2. Results from indenter material testing and model compression simulation for fibrosis and reference gels.

Liver Number	Ishak Fibrosis Grade	Indenter Test Modulus (kPa) (Fibrosis)	Model - Compression		Indenter Percent of Model Modulus (Fibrosis)
			Fibrosis Modulus (kPa)	Reference Modulus (kPa)	
1	2	1.57	**1.53**	**6.12**	102.1%
2	3	1.27	**1.70**	**6.52**	74.5%
3	4	1.64	**1.88**	**6.69**	87.6%
4	3	1.19	**1.53**	**6.67**	77.6%
5	3	0.85	**1.42**	**5.84**	59.9%

Table 3. Average modulus values and standard deviations from indenter material testing and model compression simulation for control gel.

	Indenter Test Modulus (kPa)	Model – Compression Modulus (kPa)
Control Average (kPa)	0.69 +/- 0.06	0.65 +/- 0.13
Normal Average (kPa)	0.55 +/- 0.04	0.55 +/- 0.05
Average Non-Diseased Modulus (kPa)	0.62 +/- 0.09	0.59 +/- 0.09

A correspondence is suggested between indenter and model-based assays of modulus, as can be seen in Figure 9 and in the last column of Table 2. Figure 9 plots the model-based modulus for each fibrotic liver versus the indenter test modulus. A general trend exists between the two sets of measures, where as the indenter modulus increases, so does the model modulus. This is again represented in the last column of Table 2, which gives the indenter modulus as a percentage of the model modulus. With exception of the liver 1 measurement, the modulus as measured by the indenter is consistently lower than the model modulus and represents an approximate mean of 74.0%+/-10.4%. As Figure 9 indicates, a discrete least squares approximation generates a reasonably good linear fit between the two methods when the liver 1 measurement is discarded. Although the statistics do not support an outlier designation for the liver 1 measurement at this time, the difference in the correlation coefficient of Figure 9 is quite compelling. In addition, if one looks at the standard deviation of the error for each of the points from livers 2-5 for the linear fit in Figure 9, the error associated with liver 1's measurement would be greater than three standard deviations. While semi-quantitative, the data suggests that liver 1 may indeed be an outlier measurement. As sample size is increased, the relationship shown in Figure 9 may indicate that the indentation method may be used to establish ex-vivo tissue modulus values using a linear correlation. Again, this would be specific for murine systems undergoing chemically-induced fibrosis. The fact that the control/normal moduli are so similar among testing methods would indicate that factors regarding the distribution of disease may be the cause for this difference in tissue measurement in the fibrotic livers. Figure 10 provides a visual comparison of the results from each testing methodology. Figure 10a shows the indenter modulus for each liver, while figure 10b shows the model-calculated modulus. The horizontal dashed line in each of these figures designates the respective mean non-diseased liver measurement.

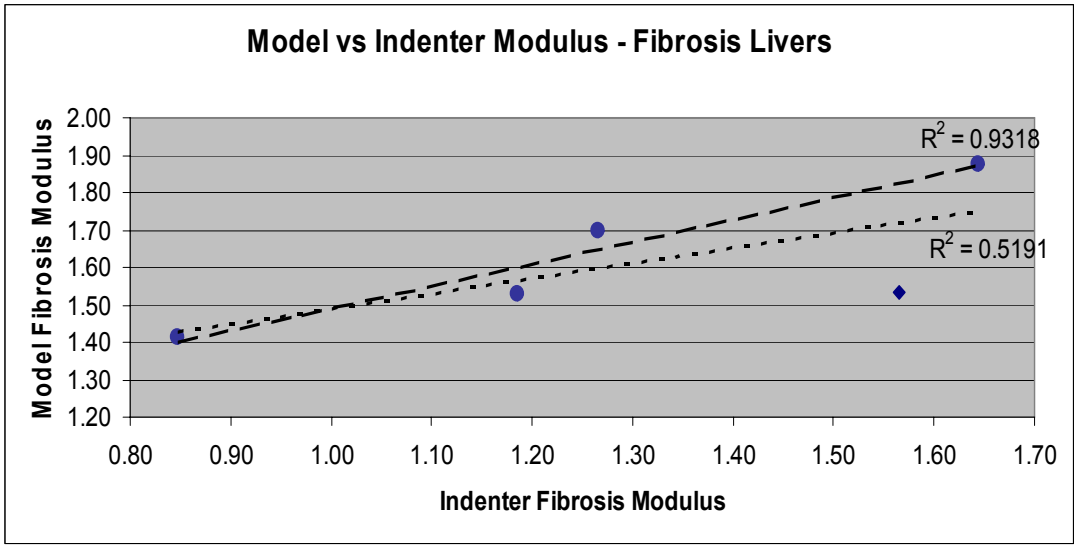

Figure 9. Model modulus as a function of indenter modulus. The diamond-shaped point represents liver 1, which is considered to be an outlier point. A fit for the relationship between indenter modulus and model modulus with all five data points gives the small-dashed line, with a correlation coefficient (R) of 0.721. If the data point from liver 1 is removed, the linear regression becomes the large dashed line, with correlation coefficient of 0.965, indicating a relationship between the two sets of modulus values.

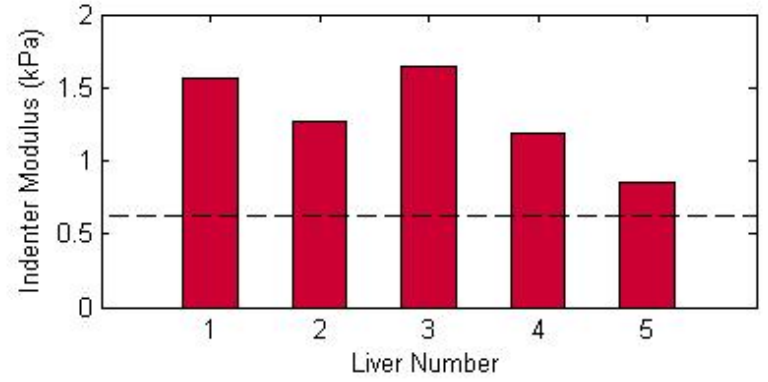

a

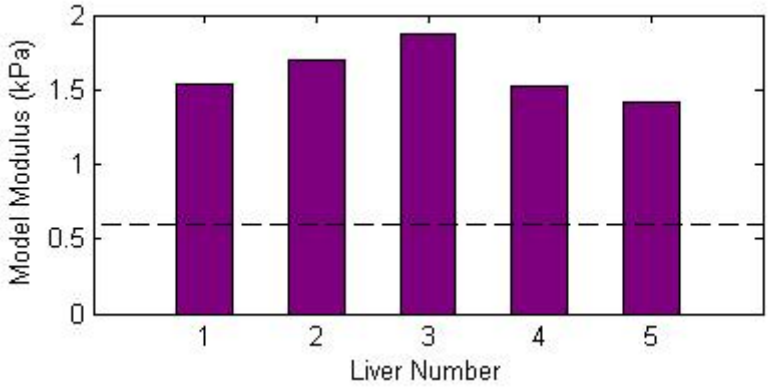

b

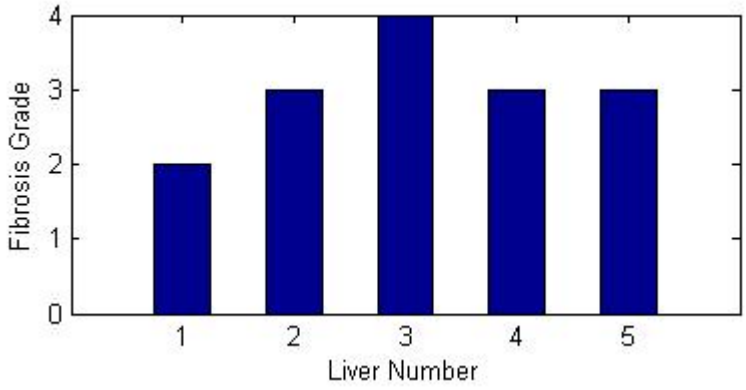

c

Figure 10. Bar graphs representing the (a) indenter material testing modulus values, (b) model compression modulus values, and (c) Ishak grade for the five fibrotic livers evaluated during the course of the research. The dashed lines on the indenter modulus and model modulus graphs represent the average control/normal liver value for the indenter and model modulus values, respectively.

Another evaluation of interest is the fibrosis grade versus modulus measurement which can easily be seen in Figure 10c. Table 2 shows the Ishak fibrosis grade assigned by analysis of histology slides of the fibrotic livers. The Ishak fibrosis grade varies between 0 (no disease) and 6 (cirrhosis). From Table 1, three livers were assigned a grade of 3, one a grade of 4, and one a grade of 2. All of the livers graded 3 have modulus values lower than the modulus value for the liver assigned a grade of 4. However, two of the three livers assigned a grade of 3 have a modulus value lower than the modulus of the liver assigned a grade of 2. While visually, there appears to be some correlation between model-based modulus determination and the Ishak grade, this is uncertain at this time. However, when comparing the modulus-grade correlation to that of the indenter test-grade correlation, the modulus-grade correlation appears to be somewhat more supported. More specifically, calculating the correlating coefficient between Ishak grade and indenter modulus yields a correlation coefficient of R=0.087, while the coefficient between Ishak grade and model-based modulus is R=0.674. If liver 1's measurement was eliminated from both sets, the correlation coefficient rises to R=0.832, and R=0.814, respectively, further implying that liver 1 could be an outlier.

Discussion

The polyacrylamide gel was chosen as the gel matrix based on its insensitivity to thermal fluctuations, rapid congealing properties, and stability. Agarose is a hydrogel, and the gel is solidified by cooling the components on ice. As it is exposed to room temperature for prolonged periods of time, the gel liquefies and changes properties. Polyacrylamide solidifies by way of a polymerization reaction, which limits the thermal dependence. For experimental purposes, where the gel would be exposed to room temperature for prolonged periods of time during imaging and material testing, the thermal behavior of agarose was unacceptable, eliminating it as an option.

Polyacrylamide did not exhibit the same extreme thermal dependence. Polyacrylamide could also be easily adjusted to generate a desired modulus by changing the weight percentage of the polyacrylamide added to the solution. We found that 5% polyacrylamide resulted in a gel that had an average modulus of 6.1 kPa.

Research has indicated that, in general, biological soft tissues are viscoelastic in nature, and, therefore, research commonly utilizes cyclic compressions to estimate the viscous reaction of biological soft tissue and isolate their nature [33]. In contrast, some testing regiments institute a dwell period if they are concerned with factoring out such influences. When considering diagnostic processes such as elastography, in particular static-based methods which involve a prolonged state of compression, using the latter strategy to estimate properties would seem appropriate [34, 35]. When considering surgical loading conditions also, a static-based assessment is more suitable [27]. Thus, for compatibility reasons with research directions within our laboratory, a dwell period was instituted to factor out transient behavior and data was analyzed at these approximate steady state times. The dwell period length was chosen as 60 seconds for two reasons. First, this length of time was sufficient to approximate steady state as is indicated by Figure 8, which shows the force curve for a sample liver indentation under the protocol described above. Second, this time frame is relative to how long it takes to acquire an image in ultrasound elastography, or other elastography techniques, which is a current focus within our laboratory. There is little doubt that tissue is viscoelastic, and the force-to-displacement behavior will change with increasing load rate. However, as with any material testing protocol, the loading environment concerned with the application must be taken into account. In addition, the same dwell period was implemented for both the indenter and compression tests in order to provide uniformity to the investigation. These dwell periods may be adjusted in the future depending on the application or if certain information regarding diseased tissue can be uncovered by

looking at different loading events temporally. We should also note that a linear regression was performed on the "steady-state" data to establish stress-to-strain relationships at these time points; and in each case, a consistent correlation value of greater than 0.99 was determined thus indicating a reasonably robust analysis at this time point.

The main purpose of this research was to identify whether a gel-tissue system could be developed to measure the stiffness of an embedded piece of tissue. Though our sample number was small, and thus we cannot fully assess the accuracy of the system, we were able to generate a testing protocol that delivered reasonable results for the elastic modulus of our trial samples. In addition, a chemically-induced liver fibrosis model was used to determine whether intuitive changes in these properties could be monitored. The dual-testing method allowed for independent confirmation and may have indicated differing sensitivities in our model-based and indentation methods. More specifically, the results from Tables 2 and 3 indicate that our model-based method may be better than indentation tests for assessing fibrosis. While quantitatively limited with respect to sample size, Table 3 indicates that each method measured the same Young's modulus for the control/normal livers. This would seem to indicate that indentation and the model-based method are performing similarly. However, with the measurements associated with the fibrotic livers, the indenter estimate was consistently below that of the model-based method by approximately 26%. One of the distinct differences between the two tests is the extent of the mouse liver used within each test. The two largest lobes are used in the model-based test, while one of the smaller lobes is used for the indentation. The other distinct difference is that indentation tests are measured on the surface of a liver lobe. It is quite possible that the outer parenchymal capsule associated with the liver may not have the same degree of fibrosis as the internal regions of the organ. Any heterogeneity with respect to the fibrosis in regions near the

outer surface of the liver would inherently affect indentation tests more. The fact that the moduli values were less for these tests would be consistent with this assertion as the outer surface would be the most likely region to not have fully developed fibrosis. The model-based gel-tissue assay would be more representative of global organ fibrosis and the properties would reflect this.

It was also interesting that the histological fibrosis grading did seem to correlate with mechanical property measurements. As many will attest, histological scoring is quite subjective. In future work, we would like to automate scoring using image processing techniques and correlate that with mechanical property measurements more quantitatively. However, the results do provide some important findings. First, there is a clear difference in both histological grading, with scores ranging from 2 to 4, and their respective mechanical properties, with values ranging from 2 to 2.8 times larger for fibrotic mice. Based on this preliminary testing with normal livers, we would assert that property resolution changes of approximately 0.07 kPa and 0.25 kPa may be discernible using the indentation and model-based method, respectively (estimated as two standard deviations of the control property estimate). As expected, the indentation test would ultimately be more sensitive, but the results here indicate that the gel-tissue system may be more representative of global organ changes. While this discrepancy is important, with respect to monitoring disease, changes from the control/normal were relatively easy to capture with both methodologies. While we suggest that the sensitivity may be 0.25 kPa for the gel-tissue assay, this may be an overly conservative estimate. When observing Figures 10a-10c, it does seem as if the gel-tissue assay is tracking disease grade. Ultimately, more specimens need to be analyzed to be certain. Additionally, we could increase the sensitivity by decreasing the gel-to-tissue volume fraction to detect more subtle changes in the organ stiffness.

There are several sources of error within our techniques that reflect limitations of this protocol. All methods herein represent an *ex-vivo* methodology. Without linking the *in-vivo* and *ex-vivo* properties, it will be difficult to use this as a quantitative metric for *in-vivo* changes. Nevertheless, the protocol does represent a reasonably robust technique to monitor changes under like conditions. There are a myriad of other possible sources of error to include: segmentation, tetrahedral element choice, variability in disease model, subjectivity of disease grading, variability in pre-compression environment, etc. However, the independent method testing performed herein does provide confirmation regarding the detection of disease. The results also indicate that indentation and the gel-tissue assay may provide information regarding fibrosis at both a local and more global level. The results also seem to indicate correlation between the methods as well as qualitative agreement with disease grade. Furthermore, it should be noted that one advantage of the gel-tissue assay is it would be amenable for calibrating elastography methods and conducting controlled experiments among different modalities.

Conclusions

Our gel testing/model method yielded results that could be correlated to indenter testing of the individual liver lobes. Though one outlier is suspected in our tests, the remaining samples display a correlation between indenter modulus and model modulus for the fibrotic livers. The control/normal liver modulus values are consistent for both the model and indenter tests. However, the fibrotic livers resulted in modulus values that were consistently higher in the model calculation than in the indenter calculation. Rather than thinking this is a limitation of either theory, we hypothesize that this may be due to the indentation being performed at the liver surface, which is a region that may experience less fibrosis formation than the organ volume. The compatible measurements of the control/normal livers between indentation and model-based

method would seem to indicate this. The results from this research are not absolute, as the sample number needs to be increased. However, the goal was to identify a protocol by which the gel-embedded livers could be tested, and verify whether the liver samples could be recognized within the gel matrix. Our results indicate that the liver could in fact be identified within the gel as an anomaly. In addition, the correlation between the indenter modulus and model modulus demonstrates the potential of the system to accurately characterize the liver modulus. Future work will focus on further assessment of the model's ability to accurately define the liver modulus based on tests performed with larger sample numbers. In addition, enhancements to the model regarding element-type and perhaps more complicated constitutive relations to match the transient properties would be appropriate for investigation as well as more work to increase the quantitative nature of the disease grading. Despite some limitations, the techniques and results produced herein should serve as robust framework for testing elastography techniques as well as to monitor small-animal diseases systems that affect soft tissue architecture.

CHAPTER III

FUTURE WORK

Future work for this project will be foremost focused on generating a larger sample set by which further evaluation of the testing and analysis protocol can be performed. In addition, there are couple of addendums will be made to the current system. First, the reference gels will undergo CT scanning in order to accurately represent their shape. Though it is not believed that shape inaccuracies had a significant effect on the results presented, the reference CTs will add accuracy to the investigation. Other possible changes to the current approach are with respect to the model. The current finite element mesh consisted of tetrahedral elements. Surface elements, which are subject to the boundary conditions, are 75 percent constrained since the motion of three of the four nodes is described by the boundary condition. This has been shown to cause an artificial stiffening of the mesh. Brick elements, on the other hand, are only 50 percent constrained. Other types of elements are also less constrained, which reduces or eliminates the stiffening effect. Thus, the implementation of another type of element may be of interest to evaluate this effect, since our property of concern is a measure of the liver stiffness. Additionally, a nonlinear model could be implemented to further address the nonlinear nature of the tissue. Our current evaluation technique does appear to eliminate the need for a nonlinear model, but if further analysis with more samples indicates the need for a more refined tissue model, this could be addressed. Another future addition to the analysis procedure is a quantitative assessment of the fibrosis grade. We plan to develop an automated system to quantify the amount of fibrosis present in the histological slides based upon the percent of stained area.

The most significant addition to the research will be the addition of ultrasound evaluation to the process. Previous work included ultrasound evaluation of the gel samples, but the resulting data were not useful, which we believe was a result of our approach combined with an incomplete evaluation of the capabilities of the US system. A device was generated that allowed successive compression of the gel with ultrasound data collection occurring between incremental compressions. However, the compression was occurring in the far-field of the ultrasound, which resulted in very noisy data that could not be analyzed. Testing is underway to further understand the ultrasound device, and, if that does not resolve the issue with the compression device, then a new device may be created. The device includes a load cell which measures the force applied during the gel compression, and a short program is being generated in Labview to allow collection of the data. This will precipitate correlation of the ultrasound data to the material testing data and model results. It will also ease the possible application of elastography to the ultrasound data, as we will have values for both applied force and displacement to correlate with the ultrasound data. With these measured values, the possibility exists for inversion of the displacement field generated by elastography, which would allow direct assessment of the tissue elastic modulus.

REFERENCES

1. National Institute on Alcohol Abuse and Alcoholism, o.t.N.I.H. *Age-specific number of deaths for all cirrhosis by race, Hispanic origin, and sex, United States, 1970–2003.* 2006 [cited 2007 March 15]; Available from: http://www.niaaa.nih.gov/Resources/DatabaseResources/QuickFacts/Liver/cirmrt2a.htm.

2. Fowell, A.J. and J.P. Iredale, *Emerging therapies for liver fibrosis.* Digestive Diseases, 2006. **24**(1-2): p. 174-183.

3. Friedman, S.L., *Scarring in alcoholic liver disease - New insights and emerging therapies.* Alcohol Health & Research World, 1997. **21**(4): p. 310-+.

4. Miller, K. and K. Chinzei, *Mechanical properties of brain tissue in tension.* J Biomech, 2002. **35**(4): p. 483-90.

5. Miller, K. and K. Chinzei, *Constitutive modelling of brain tissue: experiment and theory.* Journal of Biomechanics, 1997. **30**(11/12): p. 1115-1121.

6. Carter, F.J., et al., *Measurements and modelling of the compliance of human and porcine organs.* Med Image Anal, 2001. **5**(4): p. 231-6.

7. Chen, E.J., et al., *Young's modulus measurements of soft tissues with application to elasticity imaging.* Ieee Transactions on Ultrasonics Ferroelectrics and Frequency Control, 1996. **43**(1): p. 191-194.

8. Miller, K., *Biomechanics of soft tissues.* Med Sci Monit, 2000. **6**(1): p. 158-67.

9. Beaugrand, M., *How to assess liver fibrosis and for what purpose?* Journal of Hepatology, 2006. **44**(3): p. 444-445.

10. Yeh, W.C., et al., *Elastic modulus measurements of human liver and correlation with pathology.* Ultrasound Med Biol, 2002. **28**(4): p. 467-74.

11. Gomez-Dominguez, E., et al., *Transient elastography: a valid alternative to biopsy in patients with chronic liver disease.* Aliment Pharmacol Ther, 2006. **24**(3): p. 513-8.

12. Sandrin, L., et al., *Transient elastography: a new noninvasive method for assessment of hepatic fibrosis.* Ultrasound Med Biol, 2003. **29**(12): p. 1705-13.

13. Klatt, D., et al., *In vivo determination of hepatic stiffness using steady-state free precession magnetic resonance elastography.* Investigative Radiology, 2006. **41**(12): p. 841-848.

14. Kruse, S.A., et al., *Tissue characterization using magnetic resonance elastography: preliminary results.* Physics in Medicine and Biology, 2000. **45**(6): p. 1579-1590.

15. Rouviere, O., et al., *MR elastography of the liver: Preliminary results.* Radiology, 2006. **240**(2): p. 440-448.

16. Corpechot, C., et al., *Assessment of biliary fibrosis by transient elastography in patients with PBC and PSC.* Hepatology, 2006. **43**(5): p. 1118-1124.

17. Huwart, L., et al., *Liver fibrosis: non-invasive assessment with MR elastography.* Nmr in Biomedicine, 2006. **19**(2): p. 173-179.

18. Cotin, S., H. Delingette, and N. Ayache, *Real-time elastic deformations of soft tissues for surgery simulation.* IEEE Transactions on Visualization and Computer Graphics, 1999. **5**(1): p. 62-73.

19. Cotin, S., et al., *Geometric and physical representations for a simulator of hepatic surgery.* Stud Health Technol Inform, 1996. **29**: p. 139-51.

20. Marescaux, J., et al., *Virtual reality applied to hepatic surgery simulation: The next revolution.* Annals of Surgery, 1998. **228**(5): p. 627-634.

21. Soler, L., et al., *An automatic virtual patient reconstruction from CT-scans for hepatic surgical planning.* Stud Health Technol Inform, 2000. **70**: p. 316-22.

22. Donnelly, B.R. and J. Medige, *Shear properties of human brain tissue.* Journal of Biomechanical Engineering-Transactions of the Asme, 1997. **119**(4): p. 423-432.

23. Krouskop, T.A., et al., *Elastic moduli of breast and prostate tissues under compression.* Ultrason Imaging, 1998. **20**(4): p. 260-74.

24. Kiss, M.Z., T. Varghese, and T.J. Hall, *Viscoelastic characterization of in vitro canine tissue.* Physics in Medicine and Biology, 2004. **49**(18): p. 4207-4218.

25. Ishak, K., et al., *Histological grading and staging of chronic hepatitis.* Journal of Hepatology, 1995. **22**: p. 696-699.

26. Stevanovic, M., M. Yovanovich, and J.R. Culham, *Modeling contact between rigid sphere and elastic layer bonded to rigid substrate.* IEEE Trans on Components and Package Technologies, 2001. **24**(2): p. 207-212.

27. Cash, D.M., et al., *Image-guided liver surgery: Concepts and initial clinical experiences.* Journal of Gastrointestinal Surgery, 2006. **(in press)**.

28. Cash, D.M., et al., *Compensating for intraoperative soft-tissue deformations using incomplete surface data and finite elements.* Ieee Transactions on Medical Imaging, 2005. **24**(11): p. 1479-1491.

29. Miga, M.I., et al., *In vivo quantification of a homogeneous brain deformation model for updating preoperative images during surgery.* IEEE Transactions on Biomedical Engineering, 2000. **47**(2): p. 266-273.

30. Miga, M.I., et al., *Model-updated image guidance: Initial clinical experiences with gravity-induced brain deformation.* IEEE Transactions on Medical Imaging, 1999. **18**(10): p. 866-874.

31. Bramley, R. and X. Wang. *SPLIB: A library of iterative methods for sparse linear system*. [Technical Report] 1995 [cited.

32. Sullivan, J.M., G. Charron, and K.D. Paulsen, *A three-dimensional mesh generator for arbitrary multiple material domains.* Finite Elements in Analysis and Design, 1997. **25**(3-4): p. 219-241.

33. Wang, B., et al., *An experimental study on biomechanical properties of hepatic tissue using a new measuring method* Biomed Mat Eng, 1992. **2**(3): p. 133-138.

34. Washington, C.W. and M.I. Miga, *Modality independent elastography (MIE): A new approach to elasticity imaging.* Ieee Transactions on Medical Imaging, 2004. **23**(9): p. 1117-1128.

35. Miga, M.I., et al., *Model-updated image guidance: Initial clinical experiences with gravity-induced brain deformation.* Ieee Transactions on Medical Imaging, 1999. **18**: p. 866-874.